

INSTITUT NATIONAL DE RECHERCHE EN INFORMATIQUE ET EN AUTOMATIQUE

Remarks on the stability of Cartesian PMLs in corners

Eliane Bécache — Andrés Prieto

N° 7620

Mai 2011

Computational models and simulation



ISSN 0249-6399 ISRN INRIA/RR--7620--FR+ENG

INSTITUT NATIONAL
DE RECHERCHE
EN INFORMATIQUE
ET EN AUTOMATIQUE

INRIA

centre de recherche
PARIS - ROCQUENCOURT

Remarks on the stability of Cartesian PMLs in corners

Eliane Bécache *, Andrés Prieto†

Theme : Computational models and simulation
Équipe-Projet Poems

Rapport de recherche n° 7620 — Mai 2011 — 18 pages

Abstract: This work is a contribution to the understanding of the question of stability of Perfectly Matched Layers (PMLs) in corners, at continuous and discrete levels. First, stability results are presented for the Cartesian PMLs associated to a general first-order hyperbolic system. Then, in the context of the pressure-velocity formulation of the acoustic wave propagation, an unsplit PML formulation is discretized with spectral mixed finite elements in space and finite differences in time. It is shown, through the stability analysis of two different schemes, how a bad choice of the time discretization can deteriorate the CFL stability condition. Some numerical results are finally presented to illustrate these stability results.

Key-words: PML, perfectly matched layers, absorbing layers, stability, finite elements, finite differences, CFL condition

* eliane.becache@inria.fr, POEMS (CNRS:UMR 7231 - ENSTA - INRIA Rocquencourt), INRIA, Domaine de Voluceau-Rocquencourt, BP 105, F-78153 Le Chesnay Cédex

† andres.prieto@usc.es, Departamento de Matemática Aplicada, Universidade de Santiago de Compostela, 15782 Santiago de Compostela, Spain

Centre de recherche INRIA Paris – Rocquencourt
Domaine de Voluceau, Rocquencourt, BP 105, 78153 Le Chesnay Cedex
Téléphone : +33 1 39 63 55 11 — Télécopie : +33 1 39 63 53 30

Remarques sur la stabilité des PMLs Cartésiennes dans les coins

Résumé : Ce travail est une contribution à la compréhension de la question de la stabilité des couches absorbantes parfaitement adaptées (PMLs) dans les coins, aux niveaux continu et discret. Des résultats de stabilité sont d'abord présentés pour des PMLs Cartésiennes associées à un système hyperbolique de premier ordre général. Puis, dans le cadre de la formulation du premier ordre pression-vitesse de l'équation des ondes acoustiques, une formulation non splittée des PMLs est discrétisée par des éléments finis mixtes spectraux en espace et des différences finies en temps. On montre, à travers l'analyse de stabilité de deux schémas, comment un mauvais choix pour la discrétisation en temps peut détériorer la condition de stabilité CFL. Ces résultats de stabilité sont illustrés par des expériences numériques.

Mots-clés : PML, couches absorbantes parfaitement adaptées, stabilité, éléments finis, différences finies, condition CFL

1 Introduction

The Perfectly Matched Layers (PML) technique, introduced in 1994 by Bérenger [12] for electromagnetic problems, is considered as an efficient tool to simulate numerically wave propagation problems stated in unbounded domains. In fact, during the last decade, this technique has been intensively applied in a wide range of areas (acoustic and electromagnetic problems [15, 16, 29, 30, 33, 36], elastodynamics [6, 7, 9, 17], aeroacoustics [4, 5, 18, 23–26, 28] among others).

The mathematical analysis of the well-posedness and stability of the continuous PML models (both in the original split formulation and in unsplit formulations) have been addressed in several works. Let us cite e.g. [1, 2, 27, 31] for the well-posedness analysis and [9–11, 26] for the stability analysis. It is now well-known that the original split PML model, as well as unsplit PML models, are (at least weakly) stable if the original physical model is isotropic. However, if the physical model is anisotropic then the PML technique can lead to unstable behaviors (see [9] for more details).

On the other hand, a natural question is the analysis of the stability of fully discrete schemes used for discretizing PMLs. In [10], this question has been considered for the discretization of isotropic Maxwell's equations. Precisely, it is shown that the Yee scheme, applied for discretizing both the split and the unsplit PMLs, is stable under the standard CFL stability condition. This result is obtained for a layer in only one direction. When considering Cartesian PMLs with layers in two (or three) directions, it is then natural to address the question of stability in corners. It is well known that this question is delicate for Absorbing Boundary Conditions (ABCs) and has been considered by several authors (e.g., [19, 32], and [22] where long time instabilities for high order ABCs are mentioned).

The main goal of the present paper is to study if instabilities could be generated from the corner PML domains in 2D, as it is the case for some ABCs in corners. The first result is that, on the continuous level, PML corners are always stable (even in anisotropic models assuming that the PML parameters for each direction are constant and equal). On the discrete level, it is shown that instabilities are related to an inadequate time discretization of the auxiliary differential equations in the Cartesian PML formulation. In fact, in the context of the isotropic acoustic model, we analyze two different time discretizations whose CFL stability conditions are different only in the corner domains. Although both discrete scheme are consistent with the continuous model, only one has a CFL condition independent of the PML parameters, which coincides with the standard CFL of the scheme in the physical domain.

Following is the outline of the paper. In Section 2, we describe the split Bérenger's PML formulation, written in Cartesian coordinates for a general first order hyperbolic system in two dimensions. We focus our attention on the equation system stated only in a corner domain. It is shown that, in contrast to a layer in only one direction, PMLs are always stable in a corner, at least for a constant damping factor. In particular, it means that, even for anisotropic models, the split PMLs are stable at the continuous level.

Section 3 is devoted to the introduction of a model problem, the two dimensional wave equation, written as a first-order pressure-velocity system. The PML model considered here is the Zhao-Cangellaris unsplit formulation. Again, if the PML coefficients are assumed constant in the corner domain (but possibly different), it is shown, via energy estimates, that the continuous model is stable.

The spatial semi-discretization, presented in Section 4, is done with a spectral mixed finite element method based on a quadrilateral mesh, used in [20].

Section 5 is devoted to the time discretization, using explicit second-order finite differences. We first consider the scheme used in [20]. A stability analysis of the scheme shows that the CFL condition is deteriorated in the PML corner, when compared to the CFL condition inside the fluid domain, the deterioration depending (in particular) on the damping factor. In order to avoid this, a new discretization in time in the PML corner is proposed, for which it is shown that the CFL condition remains the same as in the fluid domain. These results are illustrated in Section 6 with numerical simulations.

2 Stability of Bérenger's splitted PMLs in corners for a general hyperbolic system

Notation. Through the rest of the paper, standard notations about functional Sobolev spaces are used without explicit definitions, $\|\cdot\|_{L^2}$ and $(\cdot,\cdot)_{L^2}$ denote respectively the L^2-norm and the L^2-inner product.

In [17], the authors have shown how to design a splitted PML model, for a general first-order hyperbolic system. This construction has been applied in [9] for analyzing the well-posedness and the stability of a layer in one direction. In this section, we focus on the PML equations written in a corner domain. Following [9, 17], we consider the first-order hyperbolic general Cauchy problem in the two dimensional free space:

$$\begin{aligned}&\partial_t U - A_x \partial_x U - A_y \partial_y U = 0,\\ &U(.,0) = U^0,\end{aligned}$$

where U is a m dimensional real-valued vector function $U : (x, y, t) \in \mathbb{R}^2 \times \mathbb{R}^+ \mapsto U(x, y, t) \in \mathbb{R}^m$, A_x and A_y are $m \times m$ real-valued symmetric matrices, and the initial data U^0 is a m dimensional real-valued vector function $U^0 : (x, y) \in \mathbb{R}^2 \mapsto U^0(x, y) \in \mathbb{R}^m$. It is then classical to show that the solution satisfies the energy conservation

$$\frac{d}{dt} \|U\|_{L^2}^2 = 0.$$

We now introduce the splitted Bérenger's PMLs equations in Cartesian coordinates ([12, 17]) using the splitting trick for the corner domain:
Find (U^x, U^y) solution of the first-order hyperbolic system

$$\partial_t U^x + \sigma_x U^x - A_x \partial_x U = 0, \tag{1}$$
$$\partial_t U^y + \sigma_y U^y - A_y \partial_y U = 0, \tag{2}$$
$$U = U^x + U^y, \tag{3}$$
$$U^x(.,0) = (U^x)^0,\ U^y(.,0) = (U^y)^0. \tag{4}$$

It is straightforward to verify the following

Theorem 1. *If σ_x and σ_y are constant and equal to σ then the solution (U^x, U^y) of system (1)-(4) satisfies*

$$\frac{d}{dt} \|U\|_{L^2}^2 = -2\sigma \|U\|_{L^2}^2 \leq 0. \tag{5}$$

In this case, the PML corner is strongly stable in the sense that the solution can be bounded by the initial data, uniformly in time:

$$\exists C > 0, \quad \|U(t)\|_{L^2} \leq C \left\|U^0\right\|_{L^2}, \quad \forall t > 0. \tag{6}$$

Proof. Since the absorbing functions are equal, adding equations (1) and (2), and using (3), we see that U satisfies the following equation:

$$\partial_t U + \sigma U - A_x \partial_x U - A_y \partial_y U = 0. \tag{7}$$

In this case, the PML corner appears as a "classical" dissipation term. The energy identity (5) and the estimate (6) follow then easily. □

The strong stability shows in particular that the solution can not grow linearly in time, therefore there is no possible long-time instability coming from the corner, when the damping factor is the same in the two directions (contrarely to some high order ABCs [22]).

The proof of an analogous energy estimate, for non-constant and different absorbing functions σ_x and σ_y, remains open (see, for instance [10]).

Remark 1. *For several models as, for instance, Maxwell's equations or the acoustic scalar wave equation, several authors [13, 15, 16, 33, 34] derived the Bérenger's PML model in terms of a complex coordinate stretching in the frequency domain. In the time domain, this point of view leads to the construction of the so-called unsplit PMLs, which do not need the splitting of the unknowns fields, but the introduction of new additional unknowns. The main advantage of this formulation is that it preserves the spatial differential operators and consequently the original spatial discretizations developed for the physical models. The original Bérenger's PML can then be reformulated in several forms (e.g. [3, 11, 21, 35]), depending on the*

choice of the auxiliary unknowns. Note that all these formulations are "equivalent", in the sense that one can go from one set of unknowns to the other through elementary linear operations (see e.g. [8, 10] for Maxwell's equations).

But contrarily to the split PMLs, there is no way of designing unsplit PMLs (which preserve the original operator) for a general first-order hyperbolic system. However, it is straightforward to see that in the particular case of a PML corner, with $\sigma_x = \sigma_y = \sigma$, the complex coordinate stretching leads to equation (7), i.e. to the same equation as the one obtained with the splitting. In that case actually there is neither splitting anymore nor additional unknowns.

3 The model problem: unsplit PMLs for the scalar wave equation

In the rest of the paper, we focus on a model problem, the two-dimensional acoustic wave equation, written as a first-order pressure-velocity system, for which we illustrate the construction of the Cartesian unsplit PMLs at the corner and derive some energy estimates. The governing equations of the original first-order hyperbolic system in terms of pressure and velocity fields are given by

$$\frac{1}{\mu}\partial_t P = \operatorname{div} \boldsymbol{V}, \tag{8}$$

$$\rho \partial_t \boldsymbol{V} = \mathbf{grad}\, P, \tag{9}$$

where P is the pressure, $\boldsymbol{V} = (V_x, V_y)$ is the velocity, μ and ρ are the bulk modulus and the mass density respectively, which are assumed to be positive bounded functions. We denote by $c = \sqrt{\mu/\rho}$ the acoustic sound velocity. Additionally, we should include the initial data for P and V and boundary conditions for the pressure field in system (8)-(9), but in order to simplify the presentation, in the rest of the paper they will be systematically omitted.

We introduce the Cartesian unsplit PMLs at the corner following the Zhao-Cangellaris' formulation [35] (recall that the solution of the split Berenger's PML can be deduced by simple linear combinations from the solution of the unsplit formulation and conversely, see [10]):
Find $(P, P^\star, \boldsymbol{V}, \boldsymbol{V}^\star)$ such that

$$\frac{1}{\mu}\partial_t P^\star = \operatorname{div} \boldsymbol{V}^\star, \tag{10}$$

$$\rho\left(\partial_t + \sigma_x I\right) V_x = \partial_x P, \tag{11}$$

$$\rho\left(\partial_t + \sigma_y I\right) V_y = \partial_y P, \tag{12}$$

$$\rho \partial_t V_x^\star = \rho\left(\partial_t + \sigma_y I\right) V_x, \tag{13}$$

$$\rho \partial_t V_y^\star = \rho\left(\partial_t + \sigma_x I\right) V_y, \tag{14}$$

$$\frac{1}{\mu}\partial_{tt}^2 P^\star = \frac{1}{\mu}\left(\partial_t + \sigma_x I\right)\left(\partial_t + \sigma_y I\right) P, \tag{15}$$

satisfying the adequate initial conditions, where $\boldsymbol{V}^\star = (V_x^\star, V_y^\star)$ and I is the identity operator. In the following, we introduce the standard notation, for any arbitrary positive bounded function ν:

$$(\phi, \psi)_\nu = (\nu\phi, \psi)_{L^2}, \quad \|p\|_\nu^2 = (\nu p, p)_{L^2}.$$

Using the same arguments showed for the Maxwell's equations in [10], straightforward computations lead to the following result:

Theorem 2. *If σ_x and σ_y are constant (but eventually different), the energy*

$$\mathcal{E}_2(t) = \frac{1}{2}\left\{\left\|\partial_t^2 P^\star\right\|_{1/\mu}^2 + \left\|\partial_t^2 \boldsymbol{V}^\star\right\|_\rho^2 + \left\|\sigma_x \partial_t V_x^\star\right\|_\rho^2 + \left\|\sigma_y \partial_t V_y^\star\right\|_\rho^2\right\},$$

satisfies

$$\frac{d}{dt}\mathcal{E}_2(t) = -2\left(\sigma_x \left\|\partial_t^2 V_x^\star\right\|_\rho^2 + \sigma_y \left\|\partial_t^2 V_y^\star\right\|_\rho^2\right) \leq 0.$$

Finally, the result showed in [11] can also be obviously extended here:

Theorem 3. *If $\sigma_x = \sigma_y = \sigma$, where σ is a positive constant, we have the following identity:*

$$\frac{1}{2}\frac{d}{dt}\left\{\|P\|_{1/\mu}^2 + \|\boldsymbol{V}^\star\|_\rho^2 + \sigma^2\,\|F\|_{1/\mu}^2\right\} = -2\sigma\,\|P\|_{1/\mu}^2\,,$$

where

$$F(t) = \int_0^t P(s)ds.$$

This implies in particular the decrease of the energy of order 0:

$$\mathcal{E}_0(t) = \frac{1}{2}\left\{\|P\|_{1/\mu}^2 + \|\boldsymbol{V}^\star\|_\rho^2\right\}.$$

4 Semi-discretisation in space using a mixed spectral element method

The system (10)-(15) is approximated in space with $Q_r - Q_r^{\rm disc}$ mixed spectral elements based on hexaedral meshes, described in [14, 20]. For the sake of simplicity in its description, we first introduce the spatial discretization for the original acoustic model before applying it to the PML problem.

4.1 Spatial approximation in the fluid domain

In order to describe briefly the mixed finite elements, we first consider the approximation of the equations set in the fluid domain Ω with Dirichlet boundary conditions for the pressure field. The variational formulation of (8)-(9) is then:
Find $P \in H_0^1(\Omega), \boldsymbol{V} \in (L^2(\Omega))^2$ such that

$$\begin{aligned}
&\frac{d}{dt}(P,\varphi)_{1/\mu} = -(\boldsymbol{V}, \mathbf{grad}\,\varphi)_{L^2}, \quad \forall \varphi \in H_0^1(\Omega),\\
&\frac{d}{dt}(\boldsymbol{V},\boldsymbol{\psi})_\rho = (\mathbf{grad}\,P, \boldsymbol{\psi})_{L^2}, \quad \forall \boldsymbol{\psi} \in (L^2(\Omega))^2.
\end{aligned}$$

We introduce $\mathcal{T} = \cup_{i=1}^{N_E} K_i$ a partition of Ω with N_E quadrilateral elements, $\widehat{K} = [0,1]^2$ the unit element, and the conform mappings F_i such that $F_i(\widehat{K}) = K_i, \forall i = 1,\ldots,N_E$. We set DF_i the Jacobian matrix of F_i and its Jacobian $J_i = \det DF_i$. We finally define the approximation spaces:

$$\begin{aligned}
\mathcal{P}_{h0}^r &= \left\{\varphi \in \mathcal{C}^0(\Omega), \quad \varphi_{|K_i} \circ F_i \in Q_r(\widehat{K}), \quad \varphi = 0 \text{ on } \partial\Omega\right\},\\
\mathcal{V}_h^r &= \left\{\boldsymbol{\psi} \in (\mathrm{L}^2(\Omega))^2, \quad |J_i| DF_i^{-1} \boldsymbol{\psi}_{|K_i} \circ F_i \in (Q_r(\widehat{K}))^2\right\},
\end{aligned}$$

with $Q_r(\widehat{K})$ the set of polynomials whose degree is less or equal to r in each spatial variable. For both spaces, the interpolation points coincide with the Gauss-Lobatto quadrature points. The semi-approximate problem is then:
Find $P_h \in \mathcal{P}_{0h}^r, \boldsymbol{V} \in \mathcal{V}_h^r$ such that

$$\begin{aligned}
&\frac{d}{dt}(P_h,\varphi_h)_{1/\mu} = -(\boldsymbol{V}_h, \mathbf{grad}\,\varphi_h)_{L^2}, \quad \forall \varphi_h \in \mathcal{P}_{0h}^r,\\
&\frac{d}{dt}(\boldsymbol{V}_h,\boldsymbol{\psi}_h)_\rho = (\mathbf{grad}\,P_h, \boldsymbol{\psi}_h)_{L^2}, \quad \forall \boldsymbol{\psi}_h \in \mathcal{V}_h^r.
\end{aligned}$$

Let $\{\varphi_j : 1 \le j \le N_\mathcal{P}\}$ the finite element basis of $\mathcal{P}_{0h}^r$ and $\{\boldsymbol{\psi}_m : 1 \le m \le N_\mathcal{V}\}$ the basis functions of $\mathcal{V}_h^r$ (see [14, 20] for a more detailed definition). These basis are associated to the interpolation

points that coincide with the quadrature points of the Gauss-Lobatto quadrature formula which is exact for polynomials of degree $2r-1$. We introduce the discrete mass and stiffness matrices

$$\begin{aligned} M_{ij} &= (\varphi_i, \varphi_j)_{1/\mu}, & 1 \le i,j \le N_{\mathcal{P}}, \\ (R_x)_{jm} &= (\partial_x \varphi_j, \boldsymbol{\psi}_m)_{L^2}, & 1 \le j \le N_{\mathcal{P}},\ 1 \le m \le N_{\mathcal{V}}, \\ (R_y)_{jm} &= (\partial_y \varphi_j, \boldsymbol{\psi}_m)_{L^2}, & 1 \le j \le N_{\mathcal{P}},\ 1 \le m \le N_{\mathcal{V}}, \\ B_{ml} &= (\boldsymbol{\psi}_m, \boldsymbol{\psi}_l)_{\rho}, & 1 \le m,l \le N_{\mathcal{V}}. \end{aligned}$$

where all the integrals are computed by using the Gauss-Lobatto quadrature formula. The main advantages of this method are: (a) it provides diagonal or block diagonal mass matrices (mass lumping) ; (b) the stiffness matrices are independent of the mesh and of the physical properties of the fluid medium (gain of storage).

The semi-discretized scheme can then be written in the matrix form:

$$\frac{d}{dt} M P_h + R_x V_{x,h} + R_y V_{y,h} = 0, \tag{16}$$

$$\frac{d}{dt} B V_{x,h} = R_x^* P_h, \tag{17}$$

$$\frac{d}{dt} B V_{y,h} = R_y^* P_h, \tag{18}$$

where we identify the notations for the unknowns and their basis coordinates.

4.2 Spatial approximation in the PML corner

Coming back to the semi-discretization of the PML corner problem, we introduce some new matrices, defined for any L^1 positive function ν

$$\begin{aligned} M_{ij}^{\nu} &= (\nu\varphi_i, \varphi_j)_{1/\mu}, & 1 \le i,j \le N_{\mathcal{P}}, \\ B_{ml}^{\nu} &= (\nu\boldsymbol{\psi}_m, \boldsymbol{\psi}_l)_{\rho}, & 1 \le m,l \le N_{\mathcal{V}}. \end{aligned}$$

The semi-discretized scheme can then be written in the matricial form as:

$$\frac{d}{dt} M P_h^{\star} + R_x V_{x,h}^{\star} + R_y V_{y,h}^{\star} = 0, \tag{19}$$

$$\left(\frac{d}{dt} B + B^{\sigma_x}\right) V_{x,h} = R_x^* P_h, \tag{20}$$

$$\left(\frac{d}{dt} B + B^{\sigma_y}\right) V_{y,h} = R_y^* P_h, \tag{21}$$

$$\frac{d}{dt} B V_{x,h}^{\star} = \left(\frac{d}{dt} B + B^{\sigma_y}\right) V_{x,h}, \tag{22}$$

$$\frac{d}{dt} B V_{y,h}^{\star} = \left(\frac{d}{dt} B + B^{\sigma_x}\right) V_{y,h}, \tag{23}$$

$$\frac{d^2}{dt^2} M P_h^{\star} = \left(\frac{d^2}{dt^2} M + \frac{d}{dt} M^{\sigma_x+\sigma_y} + M^{\sigma_x\sigma_y}\right) P_h, \tag{24}$$

5 Two alternatives for the time discretization

We introduce Δt the time step and $(P_h)^n$, $(P_h^{\star})^n$, $(\boldsymbol{V}_h)^{n+\frac{1}{2}}$, $(\boldsymbol{V}_h^{\star})^{n+\frac{1}{2}})$ denote the spatial vector fields associated to the degrees of freedom of each unknown in the fully discrete problem at time $n\Delta t$ and $(n+1/2)\Delta t$, respectively. Since we work with the unsplit PML formulation, one notices that there is the second-order equation in time (24) to be discretized in the PML corner. This leads to two different second-order centered finite difference approximations in time.

Notation. In the sequel, $\|\cdot\|$ and $(\cdot \mid \cdot)$ denote respectively the Euclidian norm and its associated inner product. For any positive matrix S, we introduce the notation:

$$(U \mid V)_S = (SU \mid V) \quad ; \quad \|V\|_S^2 = (SV \mid V)$$

5.1 Time Discretization in the fluid domain

A centered second order finite difference scheme is used for the time discretization of matrix system (16)-(18) :

$$M\frac{(P_h)^{n+1}-(P_h)^n}{\Delta t} + R_x(V_{x,h})^{n+1/2} + R_y(V_{y,h})^{n+1/2} = 0,$$

$$B\frac{(V_{x,h})^{n+1/2}-(V_{x,h})^{n-1/2}}{\Delta t} = R_x^* P_h^n,$$

$$B\frac{(V_{y,h})^{n+1/2}-(V_{y,h})^{n-1/2}}{\Delta t} = R_y^* P_h^n,$$

completed with the adequate initial conditions. We recall that this scheme is stable under the CFL stability condition (e.g. [14, 20]):

$$\sup_{u\neq 0}\frac{(M^{-1}Ku \mid u)}{\|u\|^2} < \frac{4}{\Delta t^2} \Longleftrightarrow M - \frac{\Delta t^2}{4}K \text{ is positive definite,}$$

where K is the stiffness matrix defined as $K = R\mathcal{B}^{-1}R^*$, R is the $N_{\mathcal{P}} \times 2N_{\mathcal{V}}$ matrix defined as $R = (R_x\ R_y)$ and $\mathcal{B}$ is the $2N_{\mathcal{V}} \times 2N_{\mathcal{V}}$ block diagonal matrix, each block of size $N_{\mathcal{V}} \times N_{\mathcal{V}}$ being equal to B. Classically, on a regular grid, this condition is expressed as

$$C\frac{\Delta t}{h} < 1, \tag{25}$$

where C is a constant independent of h and Δt.

In a homogeneous fluid and using a regular mesh, this condition reduces to

$$\sqrt{\mu/\rho}\frac{\Delta t}{h} < cfl_{d,r},$$

where d is the dimension of the space and r is the degree of the polynomials. The constant $cfl_{d,r}$ can be related to the CFL number in dimension one (see [20]) by

$$cfl_{d,r} = \frac{cfl_{1,r}}{\sqrt{d}}. \tag{26}$$

In particular for $r = 1$, we have $cfl_{1,1} = 1$ and in dimension d we recover the classical CFL condition:

$$c\frac{\Delta t}{h} \leq \frac{1}{\sqrt{d}},$$

which is natural since the $Q_1 - Q_1^{\text{disc}}$ discretization on a regular grid is equivalent to the standard second-order finite difference scheme.

5.2 Time Discretization in the PML corner: scheme A

In this section we consider the scheme which was originally used in [20] for the time discretization of the governing equations in the PML corners. Let us first introduce some useful notations:

$$(D_{\Delta t}U)^k = (U^{k+1/2} - U^{k-1/2})/\Delta t \ ; \quad (I_{\Delta t}U)^k = (U^{k+1/2} + U^{k-1/2})/2.$$

The time approximation for (19)-(24) provided by scheme A is written as:

$$
\begin{aligned}
&M(D_{\Delta t}P_h^\star)^{n+\frac{1}{2}} + R_x(V_{x,h}^\star)^{n+\frac{1}{2}} + R_y(V_{y,h}^\star)^{n+\frac{1}{2}} = 0,\\
&B(D_{\Delta t}V_{x,h})^n + B^{\sigma_x}(I_{\Delta t}V_{x,h})^n = R_x^* P_h^n,\\
&B(D_{\Delta t}V_{y,h})^n + B^{\sigma_y}(I_{\Delta t}V_{y,h})^n = R_y^* P_h^n,\\
&B(D_{\Delta t}V_{x,h}^\star)^n = B(D_{\Delta t}V_{x,h})^n + B^{\sigma_y}(I_{\Delta t}V_{x,h})^n,\\
&B(D_{\Delta t}V_{y,h}^\star)^n = B(D_{\Delta t}V_{y,h})^n + B^{\sigma_x}(I_{\Delta t}V_{y,h})^n,\\
&M(D_{\Delta t}^2 P_h^\star)^n = M(D_{\Delta t}^2 P_h)^n + M^{\sigma_x+\sigma_y}(D_{\Delta t}I_{\Delta t}P_h)^n + M^{\sigma_x\sigma_y}P_h^n.
\end{aligned}
$$

The initial motivation of this study comes from the instabilities observed in the numerical simulations for some values of the PML parameters (see Section 6). Their origin is located in the PML corner domains (both for variable and constant σ_α, $\alpha = x, y$), and we also observed that these instabilities were removed when decreasing either Δt or the values of σ_α.

Since the question of stability for variable σ_α is an open question even for the continuous PML models, we will assume for the analysis of the schemes that σ_α are positive constants for $\alpha = x, y$ in the corner domains. Since σ_x is constant, we have $B^{\sigma_x} = \sigma_x B$ and we can define the discrete centered operator $(D_{\Delta t}^{\sigma_x}U)^k = (D_{\Delta t}U)^k + \sigma_x(I_{\Delta t}U)^k$ to approximate $\partial_t + \sigma_x I$. With these notations and assumptions, the scheme can be rewritten as:

$$
\begin{aligned}
&M(D_{\Delta t}P_h^\star)^{n+\frac{1}{2}} + R_x(V_{x,h}^\star)^{n+\frac{1}{2}} + R_y(V_{y,h}^\star)^{n+\frac{1}{2}} = 0, && (27)\\
&B(D_{\Delta t}^{\sigma_x}V_{x,h})^n = R_x^* P_h^n, && (28)\\
&B(D_{\Delta t}^{\sigma_y}V_{y,h})^n = R_y^* P_h^n, && (29)\\
&B(D_{\Delta t}V_{x,h}^\star)^n = B(D_{\Delta t}^{\sigma_y}V_{x,h})^n, && (30)\\
&B(D_{\Delta t}V_{y,h}^\star)^n = B(D_{\Delta t}^{\sigma_x}V_{y,h})^n, && (31)\\
&M(D_{\Delta t}^2 P_h^\star)^n = M\left((D_{\Delta t}^2 P_h)^n + (\sigma_x+\sigma_y)(D_{\Delta t}I_{\Delta t}P_h)^n + \sigma_x\sigma_y P_h^n\right). && (32)
\end{aligned}
$$

We can show the stability result:

Theorem 4. *Assume that σ_x and σ_y are constant and equal to σ. The discrete scheme A is stable if the matrix*

$$M - \frac{\Delta t^2}{4}K_\sigma \tag{33}$$

is positive definite, where $K_\sigma = K + \sigma^2 M$ and $K = R\mathcal{B}^{-1}R^*$.

Proof. Since the absorbing functions are equal, it is possible to rewrite the scheme as

$$
\begin{aligned}
&M(D_{\Delta t}P_h^\star)^{n+\frac{1}{2}} = R_x(V_{x,h}^\star)^{n+\frac{1}{2}} + R_y(V_{y,h}^\star)^{n+\frac{1}{2}}, && (34)\\
&B(D_{\Delta t}V_{x,h}^\star)^n = R_x^* P_h^n, && (35)\\
&B(D_{\Delta t}V_{y,h}^\star)^n = R_y^* P_h^n, && (36)\\
&M(D_{\Delta t}^2 P_h^\star)^n = M\left((D_{\Delta t}^2 P_h)^n + 2\sigma(D_{\Delta t}I_{\Delta t}P_h)^n + \sigma^2 P_h^n\right). && (37)
\end{aligned}
$$

Applying $D_{\Delta t}$ to (34), it is then easy to eliminate $\boldsymbol{V}_h^\star$ by using (35), (36), and (37), and rewrite a scheme only in terms of P_h:

$$M\left((D_{\Delta t}^2 P_h)^n + 2\sigma(D_{\Delta t}I_{\Delta t}P_h)^n + \sigma^2 P_h^n\right) + R\mathcal{B}^{-1}R^* P_h^n = 0.$$

Introducing the stiffness matrix $K_\sigma = R\mathcal{B}^{-1}R^* + \sigma^2 M$, we see that the following discrete energy

$$\mathcal{E}_{\mathrm{A},h}^{n+\frac{1}{2}} = \frac{1}{2}\left\{\left\|\frac{P_h^{n+1} - P_h^n}{\Delta t}\right\|_M^2 + (K_\sigma P_h^n \mid P_h^{n+1})\right\}$$

satisfies the identity

$$\frac{\mathcal{E}_{\mathrm{A},h}^{n+\frac{1}{2}} - \mathcal{E}_{\mathrm{A},h}^{n-\frac{1}{2}}}{\Delta t} = -2\sigma \left\| (D_{\Delta t} I_{\Delta t} P_h)^n \right\|_M^2 ,$$

and that $\mathcal{E}_{\mathrm{A},h}^n \geq 0$ if matrix (33) is positive definite. □

Let us remark that the sufficient condition stated in the above Theorem for the stability of the numerical scheme depends on the value of the absorbing function σ, which means that the CFL condition is not the same in the PML corner than in the fluid domain. More precisely, if C is the constant appearing in the CFL condition in the fluid domain (see (25)), then the stability condition in the PML corner can be expressed as

$$\Delta t^2 \left(\frac{C^2}{h^2} + \frac{\sigma^2}{4} \right) < 1 \Longleftrightarrow \frac{C\Delta t}{h} < \frac{1}{\left(1 + \dfrac{\sigma^2 h^2}{4C^2} \right)^{1/2}}, \tag{38}$$

which is more restrictive than the one in the fluid domain.

Application: homogeneous medium and approximation with second order finite differences in time and in space. We consider here an homogeneous medium and we use the lowest order mixed spectral elements for the approximation, i.e. $r = 1$, on a regular grid. The scheme can then be written as a finite difference scheme in space and time,

$$\begin{aligned}
&\frac{1}{\mu}(D_{\Delta t} P_h^\star)_{ij}^{n+\frac{1}{2}} = (D_{\Delta x} V_{x,h}^\star)_{ij}^{n+\frac{1}{2}} + (D_{\Delta y} V_{y,h}^\star)_{ij}^{n+\frac{1}{2}}, \\
&\rho (D_{\Delta t}^{\sigma_x} V_{x,h})_{i+\frac{1}{2}j}^n = (D_{\Delta x} P_h)_{i+\frac{1}{2}j}^n, \\
&\rho (D_{\Delta t}^{\sigma_y} V_{y,h})_{ij+\frac{1}{2}}^n = (D_{\Delta y} P_h)_{ij+\frac{1}{2}}^n, \\
&(D_{\Delta t} V_{x,h}^\star)_{i+\frac{1}{2}j}^n = (D_{\Delta t}^{\sigma_y} V_{x,h})_{i+\frac{1}{2}j}^n, \\
&(D_{\Delta t} V_{y,h}^\star)_{ij+\frac{1}{2}}^n = (D_{\Delta t}^{\sigma_x} V_{y,h})_{ij+\frac{1}{2}}^n, \\
&((D_{\Delta t})^2 P_h^\star)_{ij}^n = (((D_{\Delta t})^2 P_h)^n + (\sigma_x + \sigma_y)(D_{\Delta t} I_{\Delta t} P_h)^n + \sigma_x \sigma_y P_h^n)_{ij},
\end{aligned}$$

where the subscripts ij denote the degrees of freedom at nodes of coordinates $(i\Delta x, j\Delta y)$ as usual in the finite difference discretizations in the spatial variables.

The scheme in the fluid corresponds to the classical second order finite difference scheme. In the two-dimensional case, its CFL stability condition in the fluid domain corresponds to take $C = \sqrt{2}c$ in (25) and so, we obtain

$$c\Delta t < \frac{h}{\sqrt{2}}. \tag{39}$$

In the PML corner, this condition becomes

$$c\Delta t < \frac{h}{\sqrt{2}} \frac{1}{\left(1 + \dfrac{\sigma^2 h^2}{8c^2} \right)^{1/2}}. \tag{40}$$

5.3 Time discretization in the PML corner: scheme B

In this section we propose a new scheme which corresponds to another time discretization of the last second order differential equation (24):

$$
\begin{aligned}
&M(D_{\Delta t}P_h^\star)^{n+\frac{1}{2}} + R_x(V_{x,h}^\star)^{n+\frac{1}{2}} + R_y(V_{y,h}^\star)^{n+\frac{1}{2}} = 0,\\
&B(D_{\Delta t}V_{x,h})^n + B^{\sigma_x}(I_{\Delta t}V_{x,h})^n = R_x^* P_h^n,\\
&B(D_{\Delta t}V_{y,h})^n + B^{\sigma_y}(I_{\Delta t}V_{y,h})^n = R_y^* P_h^n,\\
&B(D_{\Delta t}V_{x,h}^\star)^n = B(D_{\Delta t}V_{x,h})^n + B^{\sigma_y}(I_{\Delta t}V_{x,h})^n,\\
&B(D_{\Delta t}V_{y,h}^\star)^n = B(D_{\Delta t}V_{y,h})^n + B^{\sigma_x}(I_{\Delta t}V_{y,h})^n,\\
&M(D_{\Delta t}^2 P_h^\star)^n = M(D_{\Delta t}^2 P_h)^n + M^{\sigma_x+\sigma_y}(D_{\Delta t}I_{\Delta t}P_h)^n + M^{\sigma_x\sigma_y}(I_{\Delta t}^2 P_h)^n.
\end{aligned}
$$

For constant values of the damping parameters, this scheme becomes:

$$
\begin{aligned}
&M(D_{\Delta t}P_h^\star)^{n+\frac{1}{2}} + R_x(V_{x,h}^\star)^{n+\frac{1}{2}} + R_y(V_{y,h}^\star)^{n+\frac{1}{2}} = 0, && (41)\\
&B(D_{\Delta t}^{\sigma_x}V_{x,h})^n = R_x^* P_h^n, && (42)\\
&B(D_{\Delta t}^{\sigma_y}V_{y,h})^n = R_y^* P_h^n, && (43)\\
&B(D_{\Delta t}V_{x,h}^\star)^n = B(D_{\Delta t}^{\sigma_y}V_{x,h})^n, && (44)\\
&B(D_{\Delta t}V_{y,h}^\star)^n = B(D_{\Delta t}^{\sigma_x}V_{y,h})^n, && (45)\\
&M(D_{\Delta t}^2 P_h^\star)^n = M(D_{\Delta t}^{\sigma_x}D_{\Delta t}^{\sigma_y}P_h)^n, && (46)
\end{aligned}
$$

In this scheme, the operator $(\partial_t + \sigma_x I)(\partial_t + \sigma_y I)$ appearing in (24) has been approximated by $D_{\Delta t}^{\sigma_x}D_{\Delta t}^{\sigma_y}$, which is in some sense more natural than the discretization used in (32).

We can show the stability result:

Theorem 5. *We assume that σ_x and σ_y are constants (not necessarily equal). The discrete scheme B is stable if the matrix*

$$\mathcal{B} - \frac{\Delta t^2}{4} R^* M^{-1} R \tag{47}$$

is positive definite.

Proof. We apply $D_{\Delta t}^2 I_{\Delta t}$ to (41) and multiply with $D_{\Delta t}^2 P_h^\star$:

$$\underbrace{(D_{\Delta t}I_{\Delta t}M D_{\Delta t}^2 P_h^\star \mid D_{\Delta t}^2 P_h^\star)}_{\text{(I)}} + \underbrace{(D_{\Delta t}^2 I_{\Delta t}\boldsymbol{V}_h^\star \mid R^* D_{\Delta t}^2 P_h^\star)}_{\text{(II)}} = 0.$$

We develop each term (I) and (II) and separately:

$$\text{(I)} = \frac{1}{2\Delta t}\left((D_{\Delta t}^2 P_h^\star)^{n+1} - (D_{\Delta t}^2 P_h^\star)^{n-1} \mid (D_{\Delta t}^2 P_h^\star)^n\right)_M,$$

and, since σ_x and σ_y are constants, using (46) and then (42)-(45), we obtain

$$
\begin{aligned}
\text{(II)} &= (D_{\Delta t}^2 I_{\Delta t}\boldsymbol{V}_h^\star \mid D_{\Delta t}^{\sigma_x}D_{\Delta t}^{\sigma_y}R^* P_h)\\
&= (D_{\Delta t}^2 I_{\Delta t}V_{x,h}^\star \mid D_{\Delta t}^{\sigma_x}D_{\Delta t}^{\sigma_y}B D_{\Delta t}^{\sigma_x}V_{x,h}) + (D_{\Delta t}^2 I_{\Delta t}V_{y,h}^\star \mid D_{\Delta t}^{\sigma_x}D_{\Delta t}^{\sigma_y}B D_{\Delta t}^{\sigma_y}V_{y,h})\\
&= (D_{\Delta t}^2 I_{\Delta t}V_{x,h}^\star \mid (D_{\Delta t}^{\sigma_x})^2 D_{\Delta t}V_{x,h}^\star)_B + (D_{\Delta t}^2 I_{\Delta t}V_{y,h}^\star \mid (D_{\Delta t}^{\sigma_y})^2 D_{\Delta t}V_{y,h}^\star)_B.
\end{aligned}
$$

The last two terms in (II) can be rewritten as a difference of norms. For instance, the first one leads to

$$\begin{aligned}(D^2_{\Delta t}I_{\Delta t}V^\star_{x,h}\,|\,(D^{\sigma_x}_{\Delta t})^2D_{\Delta t}V^\star_{x,h})_B &= (D^2_{\Delta t}I_{\Delta t}V^\star_{x,h}\,|\,D^3_{\Delta t}V^\star_{x,h})_B+2\sigma_x\left\|D^2_{\Delta t}I_{\Delta t}V^\star_{x,h}\right\|^2_B\\ &\quad+\sigma_x^2(D^2_{\Delta t}I_{\Delta t}V^\star_{x,h}\,|\,D_{\Delta t}I^2_{\Delta t}V^\star_{x,h})_B\\ &= \frac{1}{2\Delta t}\left(\left\|(D^2_{\Delta t}V^\star_{x,h})^{n+\frac12}\right\|^2_B-\left\|(D^2_{\Delta t}V^\star_{x,h})^{n-\frac12}\right\|^2_B\right)\\ &\quad+2\sigma_x\left\|(D^2_{\Delta t}I_{\Delta t}V^\star_{x,h})^n\right\|^2_B\\ &\quad+\frac{\sigma_x^2}{2\Delta t}\left(\left\|(I_{\Delta t}D_{\Delta t}V^\star_{x,h})^{n+\frac12}\right\|^2_B-\left\|(I_{\Delta t}D_{\Delta t}V^\star_{x,h})^{n-\frac12}\right\|^2_B.\right)\end{aligned}$$

Hence, if the discrete energy is defined by

$$\begin{aligned}\mathcal{E}^{n+\frac12}_{\mathrm{B},h} &= \frac12\left\{\left((D^2_{\Delta t}P^\star_h)^{n+1}\,|\,(D^2_{\Delta t}P^\star_h)^n\right)_M+\left\|(D^2_{\Delta t}\boldsymbol{V}^\star_h)^{n+\frac12}\right\|^2_B\right.\\ &\quad\left.+\sigma_x^2\left\|(I_{\Delta t}D_{\Delta t}V^\star_{x,h})^{n+\frac12}\right\|^2_B+\sigma_y^2\left\|(I_{\Delta t}D_{\Delta t}V^\star_{y,h})^{n+\frac12}\right\|^2_B\right\},\end{aligned}\tag{48}$$

then we have the identity

$$\frac{\mathcal{E}^{n+\frac12}_{\mathrm{B},h}-\mathcal{E}^{n-\frac12}_{\mathrm{B},h}}{\Delta t}=-2\sigma_x\left\|(D^2_{\Delta t}I_{\Delta t}V^\star_{x,h})^n\right\|^2_B-2\sigma_y\left\|(D^2_{\Delta t}I_{\Delta t}V^\star_{y,h})^n\right\|^2_B\le 0.$$

In order to point out the stability condition we finally rewrite the discrete energy (48) as

$$\begin{aligned}\mathcal{E}^{n+\frac12}_{\mathrm{B},h}&=\frac12\left\{\left\|(I_{\Delta t}D^2_{\Delta t}P^\star_h)^{n+\frac12}\right\|^2_M-\frac{\Delta t^2}{4}\left\|(D^3_{\Delta t}P^\star_h)^{n+\frac12}\right\|^2_M+\left\|(D^2_{\Delta t}\boldsymbol{V}^\star_h)^{n+\frac12}\right\|^2_B\right.\\ &\left.+\sigma_x^2\left\|(I_{\Delta t}D_{\Delta t}V^\star_{x,h})^{n+\frac12}\right\|^2_B+\sigma_y^2\left\|(I_{\Delta t}D_{\Delta t}V^\star_{y,h})^{n+\frac12}\right\|^2_B\right\}.\end{aligned}$$

Now, applying $D_{\Delta t}$ to (41), it holds

$$M(D^3_{\Delta t}P^\star_h)^{n+\frac12}=-R(D^2_{\Delta t}\boldsymbol{V}^\star_h)^{n+\frac12},$$

and so

$$\begin{aligned}\mathcal{E}^{n+\frac12}_{\mathrm{B},h}=\frac12\left\{\left\|(I_{\Delta t}D^2_{\Delta t}P^\star_h)^{n+\frac12}\right\|^2_M+\left((B-\frac{\Delta t^2}{4}R^*M^{-1}R)(D^2_{\Delta t}\boldsymbol{V}^\star_h)^{n+\frac12}\,|\,(D^2_{\Delta t}\boldsymbol{V}^\star_h)^{n+\frac12}\right)\right.\\ \left.+\sigma_x^2\left\|(I_{\Delta t}D_{\Delta t}V^\star_{x,h})^{n+\frac12}\right\|^2_B+\sigma_y^2\left\|(I_{\Delta t}D_{\Delta t}V^\star_{y,h})^{n+\frac12}\right\|^2_B\right\}.\end{aligned}$$

Finally, since the matrix (47) is assumed positive definite, we obtain $\mathcal{E}^{n+\frac12}_{\mathrm{B},h}\ge 0$ and conclude the stability of the scheme. □

Corollary 1. *If the discrete scheme B is used, then the CFL stability condition (47) holds in the PML corner and in the fluid domain.*

Proof. We recall that the CFL condition in the fluid domain is given by requiring $M-\frac{\Delta t^2}{4}R\mathcal{B}^{-1}R^*$ is definite positive whereas the stability condition in the PML corner is obtained by assuming $\mathcal{B}-\frac{\Delta t^2}{4}R^*M^{-1}R$ is definite positive.

If we denote by (λ_j,v_j), $j=1,\dots,N_{\mathcal{P}}$ the positive eigenvalues and the eigenvectors of problem

$$R\mathcal{B}^{-1}R^*v_j=\lambda_jMv_j,\qquad v_j\neq 0,\tag{49}$$

the CFL condition in the fluid domain can be expressed as $\max_j \lambda_j < \frac{\Delta t^2}{4}$. Analogously, if we denote by (μ_j, w_j), $j = 1, \ldots, 2N_{\mathcal{V}}$ the eigenvalues and the eigenvectors of problem

$$R^* M^{-1} R w_j = \mu_j \mathcal{B} w_j, \qquad w_j \neq 0, \tag{50}$$

the CFL condition in the PML corner can be expressed as $\max_j \mu_j < \frac{\Delta t^2}{4}$. Then, it is easy to show that λ_j is a nonzero eigenvalue of (49) if and only if it is also an eigenvalue of (50). In fact, let us assume that (λ_j, v_j) is an eigenvalue and eigenvector associated to (49). If we multiply (49) by $\mathcal{B}^{-1} R^* M^{-1}$ and define $w_j = \mathcal{B}^{-1} R^* v_j$, we have $\mathcal{B}^{-1} R^* M^{-1} R w_j = \lambda_j w_j$ (obviously $w_j \neq 0$ since λ_j and v_j are not null). Hence, it is clear that λ_j is also an eigenvalue of problem (50). Reciprocally, we can use analogous arguments to show the equivalence between both eigenvalue problems. Hence, $\max_j \mu_j = \max_j \lambda_j$ and consequently the two CFL conditions coincide. □

6 Numerical illustration

We consider the free propagation of waves generated by a compact supported initial condition (Ricker impulse, e.g. [20]) for the pressure field centered at the point source $(17, 17)$, a central frequency equal to 1 and a spectral ratio equal to 0.5. The computational domain is $[-2, 20]^2$ and the thickness of the Cartesian PML is 2 (so that the physical domain is $[0, 18]^2$). The physical parameters are $\rho = 1$, $\mu = 1$.

The aim of this section is to illustrate numerically the sufficient conditions stated in Theorems 4 and 5 with two different spatial discretizations. We consider a spectral finite element method based on Q_r-Lagrange rectangular piecewise continuous elements for the pressure fields P and $P^\star$ and piecewise discontinuous elements for the velocity fields $\boldsymbol{V}$ and $\boldsymbol{V}^\star$ on uniform grids. The numerical experiments are performed with $r = 1$ and $r = 5$.

Remind that the theoretical CFL condition has been established in the case of a constant absorbing function. In the following experiments, we first try to recover these results numerically for constant damping functions:

$$\sigma_x(x) = \begin{cases} 0 & \text{if} \quad x \in [0, 18] \\ \sigma & \text{otherwise} \end{cases} \quad ; \quad \sigma_y(y) = \begin{cases} 0 & \text{if} \quad y \in [0, 18] \\ \sigma & \text{otherwise} \end{cases}. \tag{51}$$

Then, we consider a quadratic damping function, i.e. we replace the constant value σ in (51) by the quadratic profile which is continuous at the inner boundary of the PML and whose upper bound is denoted by σ^*.

Second-order scheme and constant absorbing function. For $r = 1$, the positive definite condition (47) for scheme B yields to the standard CFL condition (39), which coincides with the original CFL condition for the wave equation and then is independent of the values of σ_x and σ_y. For scheme A, the CFL condition is expected to depend on the value of the absorbing function, as shown in (40).

In Figures 1 and 2 the continuous lines illustrate the theoretical CFL condition for the discrete schemes A and B, for different values of the constant absorbing function ($\sigma = 1, 10, 25$) and therefore define the boundary of the stability region. In both Figures and through the rest of this section, the markers (see the circles, triangles and squares in the plots) are located at points $(h, \Delta t)$ corresponding to the largest value of Δt for which the schemes have been checked numerically stable in practice.

In both cases (schemes A and B), the marks lie closed to the boundary of the stability region, so the numerical results confirm the predicted CFL condition. For $\sigma = 1$, the curve for scheme A is almost the same as the one for scheme B, which means that the CFL condition is very closed to the one in the physical domain, but this setup corresponds to a very low damping which in practice would require a very large PML thickness. As soon as the damping factor is large enough, one can see that the CFL condition is much more restrictive than the standard one.

Higher-order scheme and constant absorbing function. It has been shown in [20] that, for $r = 5$, $cfl_{1,5} = 0.1010$. According to (26), we thus have in 2D: $cfl_{2,5} = 0.1010/\sqrt{2}$. Therefore, since in our numerical test $c = 1$, the CFL condition for the scheme A in the corner PML domain with a constant

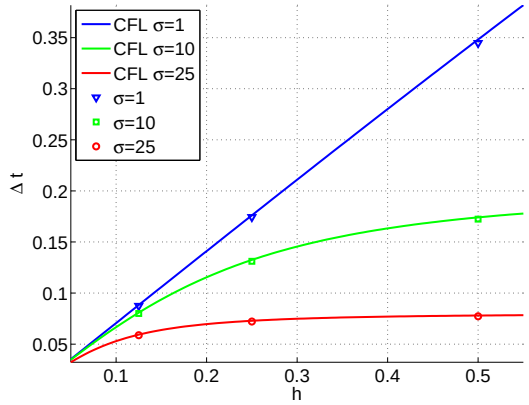


Figure 1: CFL condition for scheme A with a $Q_1 - Q_1^{\text{disc}}$ discretization and a constant absorbing function.

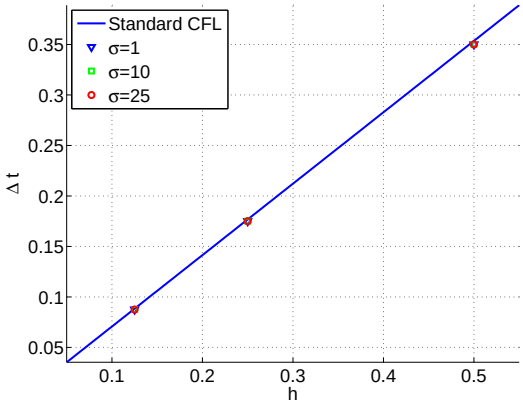


Figure 2: CFL condition for scheme B with a $Q_1 - Q_1^{\text{disc}}$ discretization and a constant absorbing function.

absorbing function σ, is given by (38) with $C = \sqrt{2}/0.1010$. In Figures 3 and 4, the results are similar to the one obtained with $r = 1$, again confirming the theoretical CFL conditions. In particular the CFL of scheme B coincides again with the standard one. However one notices that the CFL condition of scheme A is less restrictive than the one obtained with the lower order scheme.

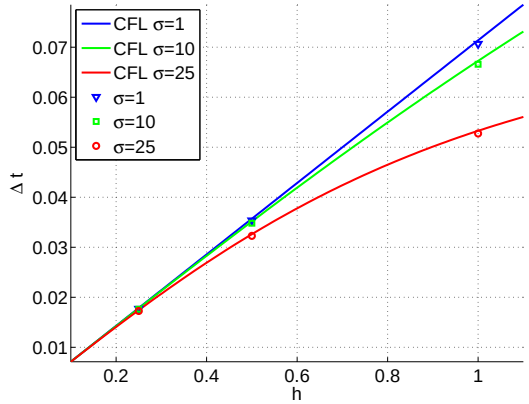


Figure 3: CFL condition for scheme A with a $Q_5 - Q_5^{\text{disc}}$ discretization and a constant absorbing function.

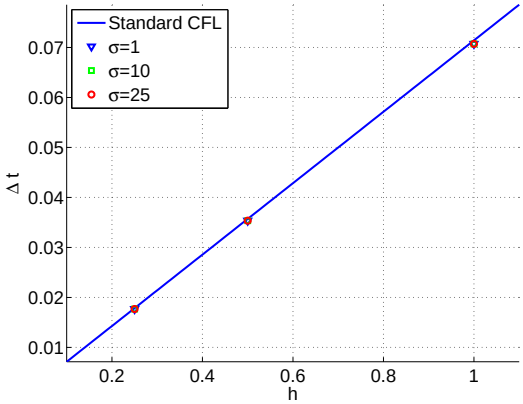


Figure 4: CFL condition for scheme B with a $Q_5 - Q_5^{\text{disc}}$ discretization and a constant absorbing function.

Quadratic absorbing function. In this paragraph, we consider a continuous quadratic absorbing function whose upper bound is given by σ^*. Notice that the theoretical CFL conditions have been obtained for a constant damping, they are therefore not valid anymore in this case. However we compare in this paragraph : (i) the stability regions obtained with the theoretical CFL corresponding to a constant damping equal to σ^* and (ii) the numerical stability region for the quadratic profile.

Figure 6 shows that the CFL condition of scheme B, obtained with $Q_1 - Q_1^{\text{disc}}$ finite elements, is still independent of σ^* and thus coincides with the standard CFL (39). These numerical results have been checked also for $Q_5 - Q_5^{\text{disc}}$ finite elements, but since they are analogous to those shown in Figure 6, they have not been included in the plots. This stability behavior, which was not guaranteed by the theoretical results, allows us to conjecture that the CFL of scheme B always remains the standard one whatever the damping profile is.

Figure 5 (resp. 7) corresponds to numerical experiments performed with scheme A and $r = 1$ (resp. $r = 5$). In both cases the numerical stability regions still depend on the absorbing profile, but this time the markers are no longer in the interior of the theoretical stability regions. This could be expected, since the theoretical CFL condition has been obtained with the maximum value of the damping profile and therefore is more restrictive than the actual CFL condition of the scheme. As in the constant case, the numerical CFL condition gets closer to the standard one, when higher-order elements are used. In practice however, since we cannot predict the CFL condition for a variable damping, scheme A is not very convenient to use and its stability condition is always more restrictive than the one of scheme B.

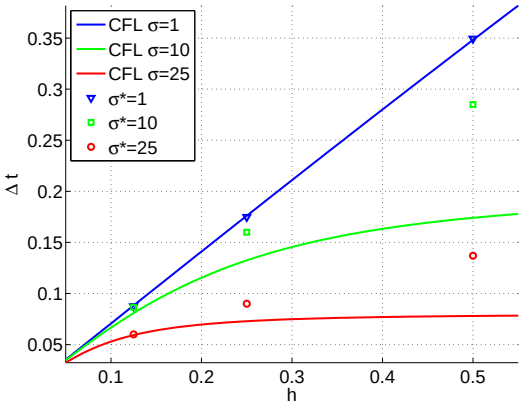


Figure 5: CFL condition for scheme A with a $Q_1 - Q_1^{\text{disc}}$ discretization and a quadratic absorbing function.

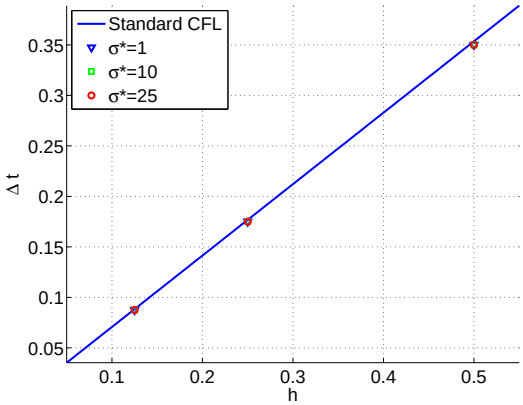


Figure 6: CFL condition for scheme B with a $Q_1 - Q_1^{\text{disc}}$ discretization and a quadratic absorbing function.

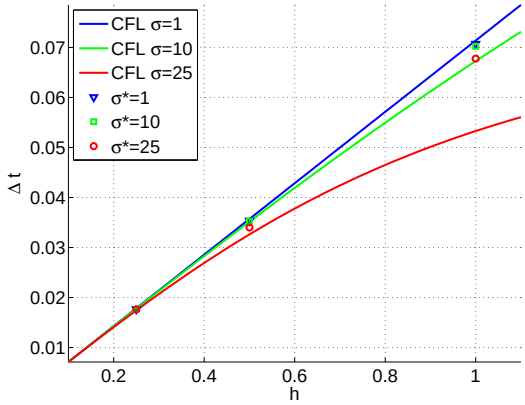


Figure 7: CFL condition for scheme A with a $Q_5 - Q_5^{\text{disc}}$ discretization and a quadratic absorbing function.

A comparison between scheme A and scheme B. Finally, to illustrate the qualitative difference between schemes A and B, we use a numerical example where scheme B is stable and scheme A is unstable. To this purpose, we present some snapshots of two numerical simulations at different time steps. We have used a $Q_1 - Q_1^{\text{disc}}$ discretization and a uniform grid with spatial sizes $\Delta x = \Delta y = 0.5$, time step $\Delta t = 0.2$. For the construction of the PML, we have used a constant absorbing functions with $\sigma = 25$. In this case, since $\Delta t < h/\sqrt{2} = 0.354$, the standard CFL holds in the physical domain and the PML corner domain for the scheme B.

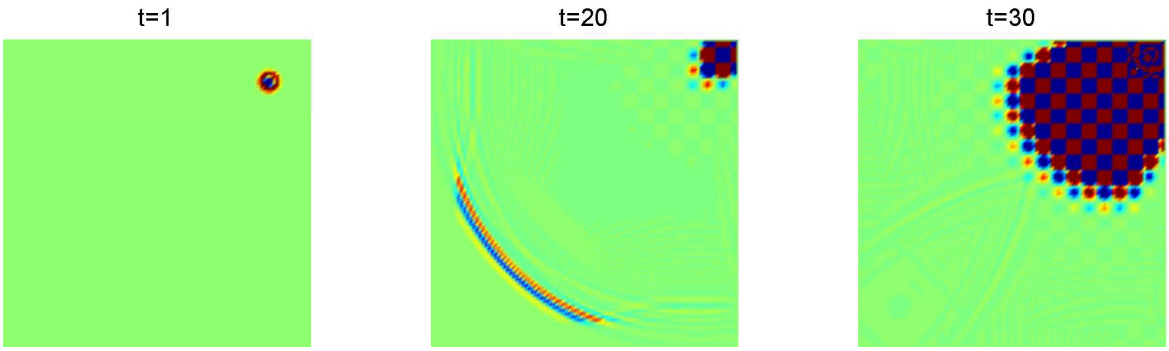


Figure 8: Snapshots at time steps $n = 1,\ 20$ and 30 for the scheme A.

As expected, whereas the scheme B remains stable (see Figure 9), an instability arises by using the scheme A (see Figure 8). Actually, the more restrictive stability condition for the corner PML, which should be used for the scheme A, is here $\Delta t < 0.078$. Figure 8 shows that the instability starts at the corner PML which is the closest one to the compact support of the initial condition. Moreover this instability arises as soon as the wave penetrates the corner PML domain and corresponds to an exponential blow up of the numerical solution.

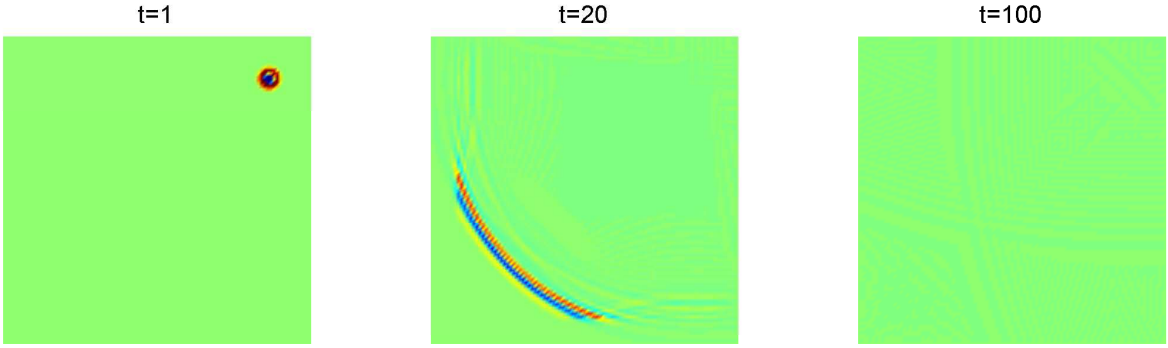


Figure 9: Snapshots at time steps $t = 1,\ 20$ and 100 for the scheme B.

Conclusion

We have emphasized that the PML models in the Cartesian corner domains are always stable and dissipative on the continuous level. However, when using the unsplit PMLs, one has to be careful on the time discretization of the equation governing the additional unknown stated in the corner domain. In this work we have shown that a bad choice for this discretization leads to a scheme which satisfies a restrictive stability condition depending on the absorbing function. The numerical solution obtained with this scheme blows up exponentially in the corner when one chooses the maximum time step allowed by the stability condition of the physical domain. This instability coming from the corner is not due to a lack of stability of the continuous model and it can be avoided with a right choice of the discretization. This new scheme (labeled as "B") leads to a CFL condition independent of the absorbing function and identical to the stability condition of the discrete scheme in the physical domain.

References

[1] S. Abarbanel and D. Gottlieb. A mathematical analysis of the PML method. *J. Comput. Phys.*, 134(2):357–363, 1997.

[2] S. Abarbanel, D. Gottlieb, and J. S. Hesthaven. Well-Posed perfectly matched layers for advective acoustics. *J. Comput. Phys.*, 154(2):266–283, 1999.

[3] S. Abarbanel, D. Gottlieb, and J. S. Hesthaven. Long Time Behavior of the Perfectly Matched Layer Equations in Computational Electromagnetics. *J. Sci. Comput.*, 17(1-4):405–422, 2002.

[4] D. Appelö, T. Hagstrom, and G. Kreiss. Perfectly matched layers for hyperbolic systems: general formulation, well-posedness, and stability. *SIAM J. Appl. Math.*, 67(1):1–23, 2007.

[5] D. Appelö and G. Kreiss. Evaluation of a well-posed perfectly matched layer for computational acoustics. In T.Y. Hou and E. Tadmor, editors, *Hyperbolic problems: Theory, Numerics, Applications*, pages 285–294, Berlin, 2003. Springer.

[6] D. Appelö and G. Kreiss. A new absorbing layer for elastic waves. *J. Comput. Phys.*, 215(2):642–660, 2006.

[7] U. Basu and Anil K. Chopra. Perfectly matched layers for transient elastodynamics of unbounded domains. *Int. J. Numer. Methods Eng.*, 59(8):1039–1074, 2004.

[8] E. Bécache. *Méthodes variationnelles, domaines fictifs et conditions aux limites artificielles pour des problèmes hyperboliques linéaires. Applications aux ondes dans les solides*. Habilitation à Diriger des Recherches, Université Paris Dauphine, 2003.

[9] E. Bécache, S. Fauqueux, and P. Joly. Stability of perfectly matched layers, group velocities and anisotropic waves. *J. Comput. Phys.*, 188(2):399–433, 2003.

[10] E. Bécache and P. Joly. On the analysis of Berenger's Perfectly Matched Layers for Maxwell's equations. *ESAIM Math. Model. Numer. Anal.*, 36(1):87–119, 2002.

[11] E. Bécache, P. G. Petropoulos, and S. D. Gedney. On the long-time behavior of unsplit perfectly matched layers. *IEEE Trans. Antennas Propag.*, 52(5):1335–1342, 2004.

[12] J. P. Bérenger. A Perfectly Matched Layer for the Absorption of Electromagnetic Waves. *J. Comput. Phys.*, 114:185–200, 1994.

[13] W. C. Chew and W. H. Weedon. A 3D perfectly matched medium from modified Maxwell's equations with stretched coordinates. *Microwave Opt. Technol. Lett.*, 7(13):599–604, 1994.

[14] G. Cohen and S. Fauqueux. Mixed finite elements with mass lumping for the transient wave equation. *J. Comput. Acous.*, 8(1):171–188, 2000.

[15] F. Collino and P. Monk. The perfectly matched layer in curvilinear coordinates. *SIAM J. Sci. Comput.*, 19(6):2061–2090, 1998.

[16] F. Collino and P. B. Monk. Optimizing the perfectly matched layer. *Comput. Methods Appl. Mech. Engrg.*, 164(1-2):157–171, 1998.

[17] F. Collino and C. Tsogka. Application of the PML absorbing layer model to the linear elastodynamic problem in anisotropic heteregeneous media. *Geophysics*, 66(1):294–307, 2001.

[18] J. Diaz and P. Joly. Stabilized perfectly matched layer for advective acoustics. In G. C. Cohen, E. Heikkola, P. Joly, and P. Neittaanmäki, editors, *Mathematical and numerical aspects of wave propagation—WAVES 2003*, pages 115–119, Berlin, 2003. Springer.

[19] B. Engquist and A. Majda. Absorbing Boundary Conditions for the Numerical Simulation of Waves. *Math. Comput.*, 31(139):629–651, 1977.

[20] S. Fauqueux. *Eléments finis mixtes spectraux et couches absorbantes parfaitement adaptées pour la propagation d'ondes élastiques en régime transitoire*. PhD thesis, Université Paris IX, 2003.

[21] S. D. Gedney. An anisotropic perfectly matched layer absorbing media for the truncation of fdtd lattices. *IEEE Trans. Antennas Propag.*, 44:1630–1639, 1996.

[22] D. Givoli, T. Hagstrom, and I. Patlashenko. Finite element formulation with high-order absorbing boundary conditions for time-dependent waves. *Comput. Methods Appl. Mech. Engrg.*, 195(29-32):3666–3690, 2006.

[23] T. Hagstrom. A new construction of perfectly matched layers for hyperbolic systems with applications to the linearized Euler equations. In G. C. Cohen, E. Heikkola, P. Joly, and P. Neittaanmäki, editors, *Mathematical and numerical aspects of wave propagation—WAVES 2003*, pages 125–129, Berlin, 2003. Springer.

[24] J. S. Hesthaven. On the analysis and construction of perfectly matched layers for the linearized Euler equations. *J. Comput. Phys.*, 142:129–147, 1998.

[25] F. Q. Hu. On absorbing boundary conditions for linearized Euler equations by a perfectly matched layer. *J. Comput. Phys.*, 129:201–219, 1996.

[26] F. Q. Hu. A stable, perfectly matched layer for linearized Euler equations in unsplit physical variables. *J. Comput. Phys.*, 173:455–480, 2001.

[27] J.-L. Lions, J. Métral, and O. Vacus. Well-posed absorbing layer for hyperbolic problems. *Numer. Math.*, 92(3):535–562, 2002.

[28] F. Nataf. A new approach to perfectly matched layers for the linearized Euler system. *J. Comput. Phys.*, 214(2):757–772, 2006.

[29] P. G. Petropoulos. Reflectionless sponge layers as absorbing boundary condition for the numerical solution of Maxwell's equations in rectangular, cylindrical, and spherical coordinates. *SIAM J. Appl. Math.*, 60(3):1037–1058, 2000.

[30] P. G. Petropoulos, L. Zhao, and A. C. Cangellaris. A reflectionless sponge layer absorbing boundary condition for the solution of Maxwell's equations with high-order staggered finite difference schemes. *J. Comput. Phys.*, 139(1):184–208, 1998.

[31] A. N. Rahmouni. *Des modèles PML bien posés pour divers problèmes hyperboliques*. PhD thesis, Université Paris Nord-Paris XIII, 2000.

[32] O. M. Ramahi. Stability of absorbing boundary conditions. *IEEE Trans. Antennas Propagation*, 47(4):593–599, 1999.

[33] C. M. Rappaport. Perfectly matched absorbing conditions based on anisotropic lossy mapping of space. *IEEE Microw. Guided W.*, 5(3):90–92, 1995.

[34] E. Turkel and A. Yefet. Absorbing PML boundary layers for wave-like equations. *Appl. Numer. Math.*, 27(4):533–557, 1998.

[35] L. Zhao and A. C. Cangellaris. A general approach for the development of unsplit-field time-domainimplementations of perfectly matched layers for FDTD grid truncation. *IEEE Microw. Guided W.*, 6(5):209–211, 1996.

[36] L. Zhao and A. C. Cangellaris. GT-PML: Generalized theory of perfectly matched layers and its application to the reflectionless truncation of finite-difference time-domain grids. *IEEE Trans. Microwave Theory Tech.*, 44(12):2555–2563, 1996.



Centre de recherche INRIA Paris – Rocquencourt
Domaine de Voluceau - Rocquencourt - BP 105 - 78153 Le Chesnay Cedex (France)

Centre de recherche INRIA Bordeaux – Sud Ouest : Domaine Universitaire - 351, cours de la Libération - 33405 Talence Cedex
Centre de recherche INRIA Grenoble – Rhône-Alpes : 655, avenue de l'Europe - 38334 Montbonnot Saint-Ismier
Centre de recherche INRIA Lille – Nord Europe : Parc Scientifique de la Haute Borne - 40, avenue Halley - 59650 Villeneuve d'Ascq
Centre de recherche INRIA Nancy – Grand Est : LORIA, Technopôle de Nancy-Brabois - Campus scientifique
615, rue du Jardin Botanique - BP 101 - 54602 Villers-lès-Nancy Cedex
Centre de recherche INRIA Rennes – Bretagne Atlantique : IRISA, Campus universitaire de Beaulieu - 35042 Rennes Cedex
Centre de recherche INRIA Saclay – Île-de-France : Parc Orsay Université - ZAC des Vignes : 4, rue Jacques Monod - 91893 Orsay Cedex
Centre de recherche INRIA Sophia Antipolis – Méditerranée : 2004, route des Lucioles - BP 93 - 06902 Sophia Antipolis Cedex

Éditeur
INRIA - Domaine de Voluceau - Rocquencourt, BP 105 - 78153 Le Chesnay Cedex (France)
http://www.inria.fr
ISSN 0249-6399